

Computational studies of the glass-forming ability of model bulk metallic glasses

Kai Zhang,¹ Minglei Wang,¹ Stefanos Papanikolaou,^{1,2} Yanhui Liu,¹ Jan Schroers,¹ Mark D. Shattuck,^{3,1} and Corey O'Hern^{1,2,4}

¹*Department of Mechanical Engineering and Materials Science,
Yale University, New Haven, Connecticut, 06520, USA*

²*Department of Physics, Yale University, New Haven, Connecticut, 06520, USA*

³*Department of Physics and Benjamin Levich Institute,*

The City College of the City University of New York, New York, New York, 10031, USA

⁴*Department of Applied Physics, Yale University, New Haven, Connecticut, 06520, USA*

(Dated: September 17, 2018)

Bulk metallic glasses (BMGs) are produced by rapidly thermally quenching supercooled liquid metal alloys below the glass transition temperature at rates much faster than the critical cooling rate R_c below which crystallization occurs. The glass-forming ability of BMGs increases with decreasing R_c , and thus good glass-formers possess small values of R_c . We perform molecular dynamics simulations of binary Lennard-Jones (LJ) mixtures to quantify how key parameters, such as the stoichiometry, particle size difference, attraction strength, and heat of mixing, influence the glass-formability of model BMGs. For binary LJ mixtures, we find that the best glass-forming mixtures possess atomic size ratios (small to large) less than 0.92 and stoichiometries near 50:50 by number. In addition, weaker attractive interactions between the smaller atoms facilitate glass formation, whereas negative heats of mixing (in the experimentally relevant regime) do not change R_c significantly. These studies represent a first step in the development of computational methods for quantitatively predicting glass-formability.

PACS numbers:

1. INTRODUCTION

When supercooled liquids are rapidly quenched at rates R exceeding a critical value R_c , crystallization is avoided, and systems form disordered solids such as bulk metallic glasses (BMGs). BMGs possess high mechanical strength and can be processed so that they display plastic [1], not brittle, response to applied deformations, which makes them desirable materials for a variety of industrial and engineering applications [2]. Avoiding crystallization in pure metals requires enormously large cooling rates in excess of 10^{12} K/s. However, bulk metallic glass-forming alloys have been developed for which the critical cooling rate is more than nine orders of magnitude lower, in the range $1 < R_c < 10^3$ K/s. Understanding the important physical quantities that determine the glass-forming ability of multi-component alloys will allow us to develop even stronger and less costly bulk metallic glasses.

Prior research suggests that multi-component metallic alloys with $T_g/T_m \gtrsim 0.67$ form BMGs, where T_g and T_m are the glass transition and melting temperature, respectively [3]. In addition, Inoue [2] has emphasized three guidelines for enabling BMG formation, rather than crystallization: 1) atomic size ratios (small relative to large) of $\alpha < 0.89$ for at least two constituents of the alloy; 2) large negative heats of mixing [4]; and 3) several atomic components. In Fig. 1, we show the distributions of the atomic size ratios and heats of mixing for common binary and ternary bulk metallic glass-forming alloys [5]. For binary systems, the most probable atomic size ratio is $\alpha \approx 0.8$ and heat of mixing is negative and roughly

6-7% of the average cohesive energy.

However, beyond these heuristic guidelines, there is no quantitative and predictive understanding of the glass-forming ability in multi-component alloys. (Note that there have been previous measurements of the critical cooling rate in binary hard-sphere systems [6, 7].) For model BMG-forming systems with attractive interactions, we do not know the dependence of the critical cooling rate on the stoichiometry, size ratios, and heats of mixing of the constituent atomic species. For example, can multi-component systems with large negative heats of mixing, but smaller atomic size mismatches possess the same glass-forming ability as systems with small negative heats of mixing but larger atomic size mismatches?

We perform molecular dynamics simulations of model glass-forming systems, binary Lennard-Jones mixtures of spherical particles, to measure the critical cooling rate as a function of the size ratio, number fraction, and interaction energy of the two particle species. We find several important results. First, the critical cooling rate decreases exponentially with the particle size ratio, $R_c \sim \exp[-C(1-\alpha)^3]$, where C depends on the number fraction of small and large particles. At a given size ratio $\alpha < 1$, the minimum critical cooling rate occurs at the number fraction corresponding to equal volumes of the large and small particles. In addition, we find that at fixed number fraction and size ratio, the critical cooling rate decreases strongly with decreasing cohesive energy ratio of the small particles relative to the large ones, $\epsilon_{BB}/\epsilon_{AA}$. In contrast, variations of the heat of mixing of the two species in the experimentally accessible range do not affect R_c significantly. Thus, we have quantified several design principles for improving glass formation in

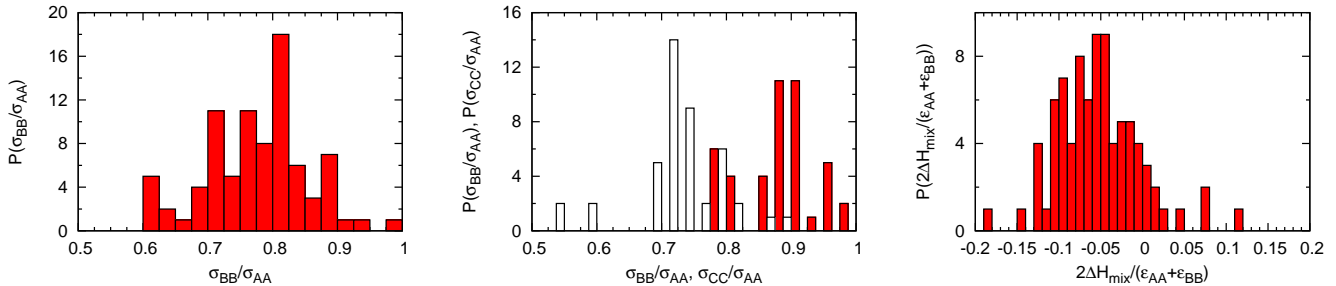


FIG. 1: (color online) (left) Probability distribution $P(\sigma_{BB}/\sigma_{AA})$ of atomic size ratios (with $\sigma_{BB} < \sigma_{AA}$) in binary bulk metallic glasses [5]. (middle) Probability distributions of atomic size ratios $P(\sigma_{BB}/\sigma_{AA})$ (shaded) and $P(\sigma_{CC}/\sigma_{AA})$ (white) (with $\sigma_{CC} < \sigma_{BB} < \sigma_{AA}$) in ternary BMGs [5]. (right) Probability distribution of the heats of mixing ΔH_{mix} relative to the average cohesive energy $(\epsilon_{AA} + \epsilon_{BB})/2$ in binary BMGs [4, 5].

binary mixtures.

2. SIMULATION METHODS

We perform constant number, volume, and temperature (NVT) molecular dynamics (MD) simulations of binary Lennard-Jones (LJ) mixtures of $N = N_A + N_B$ spherical particles with the same mass m , but different diameters σ_{AA} and σ_{BB} , in periodic cubic cells with volume $V = L^3$. The particles interact pairwise via the LJ potential

$$u(r_{ij}) = 4\epsilon_{ij} \left[\left(\frac{\sigma_{ij}}{r_{ij}} \right)^{12} - \left(\frac{\sigma_{ij}}{r_{ij}} \right)^6 \right], \quad (1)$$

where $i, j \in \{A, B\}$, B indicates the smaller particle, $\sigma_{ij} = (\sigma_{ii} + \sigma_{jj})/2$ unless otherwise specified, and ϵ_{AA} and ϵ_{BB} represent the cohesive energies for the A and B particles, respectively. We quantify the heat of mixing using $\Delta H_{\text{mix}} = (\epsilon_{AA} + \epsilon_{BB})/2 - \epsilon_{AB}$. We employ the shifted-force version of the LJ potential (Eq. 1) so that the pair potential and force vanish for separations beyond the cutoff distance $r_{\text{cut}} = 3.5\sigma_{ij}$ [8]. Energies, lengths, timescales, and temperatures are given in units of ϵ_{AA} , σ_{AA} , $\sigma_{AA}\sqrt{m/\epsilon_{AA}}$, and ϵ_{AA}/k_B , respectively, where the Boltzmann constant k_B is set to unity.

We study the glass-forming ability of binary LJ mixtures at fixed packing fraction $\phi = N\sigma_{AA}^3(1 + f_B(\alpha^3 - 1))/6V = 0.5236$ as a function of the number fraction $f_B = N_B/N$, particle size ratio $\alpha = \sigma_{BB}/\sigma_{AA}$, relative cohesive energy $\epsilon_{BB}/\epsilon_{AA}$, and heat of mixing ΔH_{mix} . We only show results for $0.92 \leq \alpha \leq 1$ for which solid solutions with FCC crystal structures are the equilibrium phase [9]. We initialize the systems at high temperature $T_0 = 2.0$, using the Nosé-Hoover thermostat [10, 11], and then thermally quench the systems exponentially, $T(t) = T_0 e^{-Rt}$, from T_0 to $T_f = 10^{-2}$ at various rates R over four orders of magnitude. (In Appendix A, we show that our results are not sensitive to the choice of the thermostat and the form of the cooling schedule.)

Following the thermal quenches to T_f , we characterize

the structural properties of the system by measuring several quantities: 1) the local and global bond orientational order parameters [12–14]

$$Q_6^l = \left(\frac{4\pi}{13} \sum_{m=-6}^6 \frac{1}{N} \sum_{i=1}^N \frac{1}{n_i} \left| \sum_{j=1}^{n_i} Y_6^m(\theta_{ij}, \phi_{ij}) \right|^2 \right)^{1/2} \quad (2)$$

$$Q_6^g = \left(\frac{4\pi}{13} \sum_{m=-6}^6 \left| \frac{1}{N} \sum_{i=1}^N \frac{1}{n_i} \sum_{j=1}^{n_i} Y_6^m(\theta_{ij}, \phi_{ij}) \right|^2 \right)^{1/2}, \quad (3)$$

where θ_{ij} and ϕ_{ij} are the axial and polar angles between each particle i and its neighbors j , Y_6^m are spherical harmonics of degree 6 and order m , and n_i is the number of nearest neighbors of particle i within a cutoff distance of $1.5\sigma_{ij}$; 2) local bond orientational order position correlation function

$$G_6(r) = \frac{4\pi}{13} \sum_{m=-6}^6 \frac{\left| \sum_i \sum_{j \neq i} q_{6m}(\vec{r}_i) q_{6m}(\vec{r}_j) \delta(\vec{r} - \vec{r}_{ij}) \right|}{g(r)}, \quad (4)$$

where $g(r) = \sum_i \sum_{j \neq i} \delta(\vec{r} - \vec{r}_{ij})$ is the radial distribution function and $q_{6m}(\vec{r}_i) = n_i^{-1} \sum_{j=1}^{n_i} Y_6^m(\theta_{ij}, \phi_{ij})$; and 3) the crystal domain size. These structural quantities are averaged over at least 96 independent quenching trajectories. (In Appendix B, we compare the results using these structural quantities.) We consider system sizes from $N = 500$ to 8788 particles.

3. RESULTS

In this section, we characterize the structural properties of LJ systems thermally quenched to temperature T_f as a function of the cooling rate R . In the right inset of the left panel of Fig. 2, we show the distribution $P(Q_6^l)$ of the local bond orientational order parameter Q_6^l for monodisperse LJ systems with $N = 1372$ particles. For

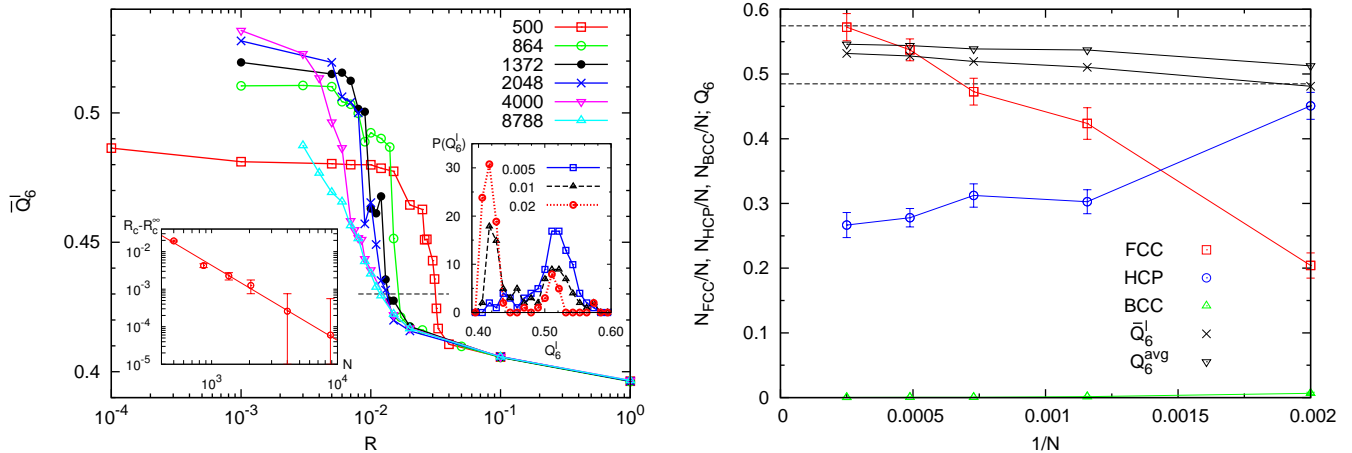


FIG. 2: (color online) (left) Median local bond orientational order parameter \overline{Q}_6^l for monodisperse Lennard-Jones (LJ) systems following thermal quenches to $T_f = 0.01$ over a range of cooling rates R for system sizes $N = 500$, 864, 1372, 2048, 4000, and 8788. The critical cooling rate R_c (defined, as discussed in the main text, as the rate at which $\overline{Q}_6^l = 0.43$ (dashed line)) approaches its large- N limit, R_c^∞ , as a power-law $R_c - R_c^\infty \sim 1/N^2$ (left inset). (right inset) The probability distribution $P(Q_6^l)$ for monodisperse LJ systems with $N = 1372$ following quenches to $T_f = 0.01$ for cooling rates $R = 0.02$ (\circ), 0.01 (Δ), and 0.005 (\square). (right) Fraction of particles that occur in HCP (\circ), FCC (\square), and BCC (Δ) crystal clusters as a function of $1/N$ for monodisperse LJ systems following a quench to T_f at cooling rate $R = 10^{-3} < R_c$. At this rate, the median local bond orientational order parameter \overline{Q}_6^l (\times) agrees with the value (∇) obtained by averaging $Q_6^l = 0.575$ for FCC and $Q_6^l = 0.485$ for HCP (dashed lines) weighted by the fraction of particles in FCC and HCP clusters in each sample.

fast cooling rates, *e.g.* $R = 0.02$, most of the quenched systems are structurally disordered, and $P(Q_6^l)$ possesses a strong peak at small $Q_6^l \sim 0.41$. In contrast, for slow cooling rates, *e.g.* $R = 0.005$, most of the quenched systems are ordered, and $P(Q_6^l)$ possesses a strong peak at a larger value of $Q_6^l \sim 0.51$. For intermediate cooling rates, the distribution $P(Q_6^l)$ becomes strongly bimodal, which indicates that the systems possess disordered as well as ordered regions. In the main panel of Fig. 2 (left), we show the median \overline{Q}_6^l versus the logarithm of the cooling rate R for several system sizes. For each system size, \overline{Q}_6^l first increases modestly with decreasing cooling rate, followed by a rapid increase at intermediate rates, and then it plateaus with further decreases. We define the critical cooling rate, R_c , as the rate at which the median local bond orientational order parameter crosses the threshold value $\overline{Q}_6^l = Q_0 = 0.43$. We chose the threshold Q_0 for several reasons: 1) Q_0 captures the steep rise in \overline{Q}_6^l with decreasing cooling rate, 2) Q_0 is in the region of Q_6^l between the two peaks in $P(Q_6^l)$ that occur at intermediate cooling rates (right inset of left panel of Fig. 2), and 3) Q_0 is a value for which $Q_6^l(R)$ becomes system size independent for intermediate and fast cooling rates.

Note that the distribution of the global bond orientational order parameter $P(Q_6^g)$ also becomes bimodal and the median \overline{Q}_6^g increases rapidly with decreasing cooling rate. (See Appendix B.) However, the global bond orientational order parameter quantifies crystallization of the *entire* system, which is influenced more by the slow dynamics of crystal growth, rather than the initial nucle-

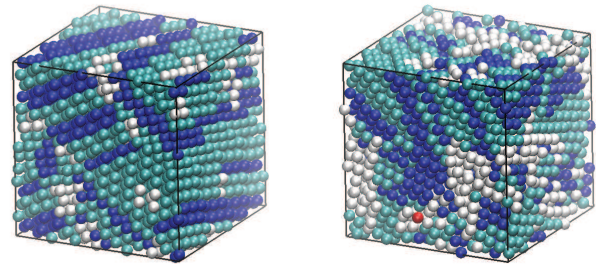


FIG. 3: (color online) Crystalline clusters obtained in monodisperse LJ systems with $N = 4000$ following thermal quenches to $T_f = 0.01$ at cooling rates $R = 10^{-3}$ (left) and 10^{-2} (right). Particles are colored according to whether they belong to FCC (cyan), HCP (blue), BCC (red), or non-crystalline (white) domains.

ation of crystalline domains.

The value of the bond orientational order parameter depends on the crystal structure that forms during the thermal quenching process. Thus, we employed a crystal analysis algorithm to identify the crystalline clusters (FCC, HCP [15], or BCC) for cooling rates $R \lesssim R_c$. For example, $Q_6^l \approx 0.575$ for an ideal face-centered cubic (FCC) structure, whereas it is ≈ 0.485 for an ideal hexagonal close packed (HCP) structure. This difference explains the increase in \overline{Q}_6^l for $R \ll R_c$ as N increases in the main panel of Fig. 2 (left). In Fig. 2 (right), we show that small systems $N \leq 500$ mainly crystallize to

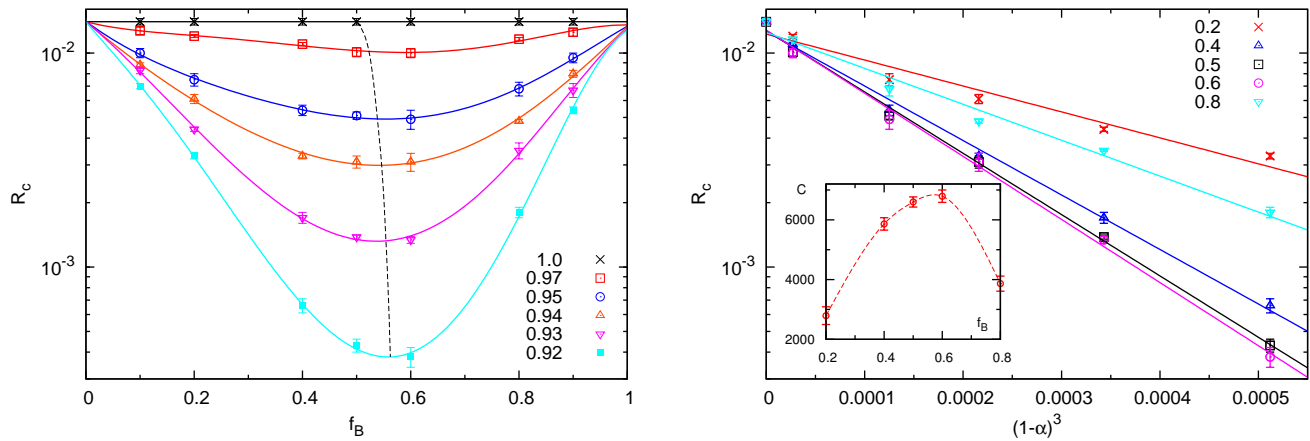


FIG. 4: (color online) (left) Critical cooling rate R_c for binary LJ mixtures with $N = 1372$ as a function of the number fraction f_B for several particle size ratios $\alpha = 1.0, 0.97, 0.95, 0.94, 0.93,$ and 0.92 . The solid lines are sixth-order least-square fits to the data for R_c . The dashed line connects the number fractions $f_B^* = 1/(1 + \alpha^3)$ at which the A and B particles occupy the same volume. (right) R_c versus $(1 - \alpha)^3$ for binary LJ mixtures with $f_B = 0.2, 0.4, 0.5, 0.6,$ and 0.8 . The error bars for R_c are determined by the cooling rate increment $\Delta R = 10^{-3}$. The inset shows the coefficient $C(f_B)$ of the exponential decay of $R_c \sim \exp[-C(1 - \alpha)^3]$.

HCP structures [16], while larger systems crystallize predominantly to FCC structures. For low cooling rates, the median local bond orientational order parameter \overline{Q}_6^l can be obtained by averaging the Q_6^l values for FCC and HCP structures weighted by the fraction of particles in FCC and HCP clusters in each sample. (See Fig. 2 (right).) We show snapshots of the thermally quenched structures for monodisperse LJ systems using two cooling rates in Fig. 3 with FCC, BCC, HCP, and non-crystalline regions shaded different colors.

We show the system-size dependence of the critical cooling rate R_c for monodisperse LJ systems in the left inset to the left panel of Fig. 2. We find that R_c decreases with increasing system size and approaches its large- N limit, $R_c^\infty \approx 0.01$, as a power law $R_c - R_c^\infty \sim 1/N^2$. It is interesting that the approach to R_c^∞ scales as $1/N^2$, which is faster than the $1/N$ scaling typical for first-order transitions. In contrast to hard-sphere systems [17], crystallization in monodisperse LJ systems is more difficult at large N . In small monodisperse LJ systems ($N \leq 500$), the critical nucleus is sufficiently large that it interacts with its periodic images [18, 19], which reduces the interfacial energy of crystal nuclei and enhances the formation of single crystals.

We now focus on binary LJ systems at fixed $N = 1372$ and cohesive energy ratio $\epsilon_{BB}/\epsilon_{AA} = 1$ and study the glass-forming ability as a function of the size ratio α and number fraction f_B . For $\alpha \lesssim 1$, the smallest $R_c(\alpha, f_B)$ (*i.e.* best glass-former) is obtained in systems with approximately equal numbers of A and B particles, $f_B^* \approx 0.5$, as shown in Fig. 4 (left). As α decreases, the minimum in $R_c(\alpha, f_B)$ deviates from $f_B^* \approx 0.5$ and follows $f_B^* = 1/(1 + \alpha^3)$ for which the A and B particles occupy the same volume (reaching $f_B^* \approx 0.56$ at

$\alpha = 0.92$). As shown in Fig. 4 (right), at each f_B , R_c decreases exponentially with decreasing size ratio, $R_c(\alpha, f_B) = R_c(1, f_B) \exp[-C(f_B)(1 - \alpha)^3]$. This result implies that R_c drops from 10^{-2} to 10^{-11} – 10^{-25} for binary systems of composition $f_B = 0.2$ – 0.8 with size ratio $\alpha = 0.8$ (the most common size ratio in binary bulk metallic glass formers), which is 9–23 orders slower than the R_c at $\alpha = 1$. We also note that for a given cooling rate R , the glass-forming regime, *i.e.* the range of number fractions for which $R > R_c$, expands with decreasing α .

For the results presented so far, we set the cohesive energy ratio $\epsilon_{BB}/\epsilon_{AA} = 1$. However, as shown in the inset to Fig. 5, the cohesive energy between like species is different for the two components for most binary bulk metallic glass formers. In Fig. 5, we show R_c as a function of $\epsilon_{BB}/\epsilon_{AA}$ for binary LJ mixtures with $N = 1372$ at fixed $f_B = 0.5$, $(\epsilon_{AA} + \epsilon_{BB})/2 = 1$, and heat of mixing $\Delta H_{\text{mix}} = 0$, assuming $\Delta H_{\text{mix}} = (\epsilon_{AA} + \epsilon_{BB})/2 - \epsilon_{AB}$ [20–22] and the mixing rules $\epsilon_{AB} = (\epsilon_{AA} + \epsilon_{BB})/2$ and $\sigma_{AB} = (\sigma_{AA} + \sigma_{BB})/2$. We find that the glass-forming ability increases (*i.e.* R_c decreases) as $\epsilon_{BB}/\epsilon_{AA}$ decreases below 1. This result is consistent with the fact that most binary glass formers with $0.8 < \alpha < 1$ possess $\epsilon_{BB}/\epsilon_{AA} < 1$ [5]. (See the inset to Fig. 5.)

Inoue’s guidelines [2] suggest that a negative heat of mixing $\Delta H_{\text{mix}} < 0$ enhances the glass-forming ability of BMGs. The rationale is that a negative heat of mixing makes the mixed and geometrically frustrated state energetically favorable compared to the phase separated state. Fig. 1 (right) shows that ΔH_{mix} is approximately 5–10% of the average cohesive energy of the two components, $(\epsilon_{AA} + \epsilon_{BB})/2$, for most binary BMGs [4, 5, 23]. However, we show in Fig. 5 that binary LJ mixtures with

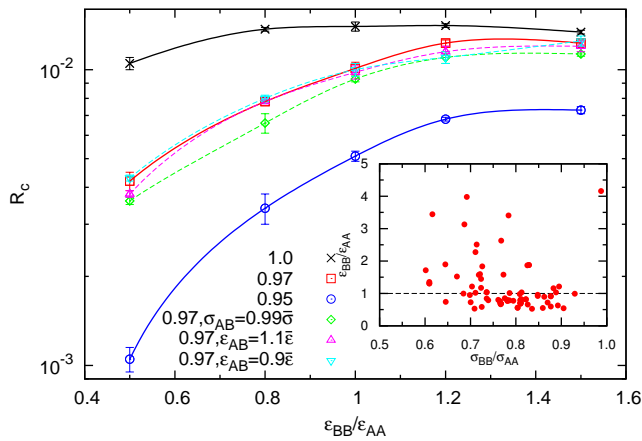


FIG. 5: (color online) Critical cooling rate R_c as a function of the cohesive energy ratio $\epsilon_{BB}/\epsilon_{AA}$ for binary LJ mixtures with $N = 1372$, number fraction $f_B = 0.5$, and size ratios $\alpha = 1.0, 0.97$, and 0.95 . The solid lines indicate results for the mixing rule $\sigma_{AB} = \bar{\sigma} \equiv (\sigma_{AA} + \sigma_{BB})/2$ and $\epsilon_{AB} = \bar{\epsilon} \equiv (\epsilon_{AA} + \epsilon_{BB})/2$. The dashed lines indicate results for positive ($\epsilon_{AB} = 0.9\bar{\epsilon}$) and negative heats of mixing ($\epsilon_{AB} = 1.1\bar{\epsilon}$) (Δ) with $\sigma_{AB} = \bar{\sigma}$ and for bond shortening $\sigma_{AB} = 0.99\bar{\sigma}$ with $\Delta H_{\text{mix}} = 0$ (\diamond). (inset) Cohesive energy ratio $\epsilon_{BB}/\epsilon_{AA}$ versus the atomic size ratio σ_{BB}/σ_{AA} for common binary metallic glass formers [5].

heats of mixing in the range $2\Delta H_{\text{mix}}/(\epsilon_{AA} + \epsilon_{BB}) = \pm 0.1$ possess the same critical cooling rate R_c as those with $\Delta H_{\text{mix}} = 0$ over the full range of size ratios studied.

Why then do most BMGs possess $\Delta H_{\text{mix}} < 0$? One possibility is that negative heats of mixing are correlated with strong bonding between atomic species, which can be modeled as bond shortening ($\sigma_{AB} < (\sigma_{AA} + \sigma_{BB})/2$) [24–26]. In Fig. 5, we show that only a 1% bond shortening, $\sigma_{AB} = 0.99(\sigma_{AA} + \sigma_{BB})/2$, can give rise to a finite decrease in the critical cooling rate R_c .

4. CONCLUSION

The glass formability of bulk metallic glass-forming alloys can be characterized by the critical cooling rate R_c , below which the system possesses crystalline domains. The best bulk metallic glasses are those with the lowest values for R_c . However, the key parameters that determine R_c are not currently known, and thus BMGs are mainly developed through a trial and error process. As a first step in computational design of BMGs, we performed molecular dynamics simulations of coarse-grained models for BMGs, binary Lennard-Jones mixtures, and measured R_c as a function of the number fraction, size ratio, relative cohesive energy, and heat of mixing of the two atomic species. We measured the local bond orientational order parameter to quantify the degree of crystallization that had occurred in systems during thermal quenches from high to low temperature over more than four or-

ders of magnitude in the cooling rate. It is known that weakly polydisperse LJ systems are poor glass-formers; we quantified this statement by showing that the critical cooling rate decreases exponentially with increasing particle size ratio α , $R_c \sim \exp[-C(1 - \alpha)^3]$. Further, at a given size ratio $\alpha < 1$, the minimum critical cooling rate occurs at the number fraction corresponding to equal volumes of the large and small particles of equal mass. In addition, we find that at fixed number fraction and size ratio, the critical cooling rate decreases strongly with decreasing cohesive energy ratio of the small particles relative to the large ones, $\epsilon_{BB}/\epsilon_{AA}$. This result may explain why most experimentally obtained binary BMGs possess $\epsilon_{BB}/\epsilon_{AA} < 1$. In contrast, variations of the heat of mixing of the two species in the experimentally accessible range (several per cent of the average cohesive energy) do not affect R_c for binary LJ mixtures significantly. However, bond shortening of only several percent relative to $\sigma_{AB} = (\sigma_{AA} + \sigma_{BB})/2$ [24–26] does give rise to significant changes in R_c . Recent experiments have suggested that negative heats of mixing are correlated with bond-shortening, which may explain why most experimentally obtained BMGs possess negative heats of mixing. In future studies, we will characterize the glass-forming ability and crystallization processes in ternary and quaternary LJ mixtures using MD simulations, energy minimization, and genetic algorithms.

Acknowledgments

We thank Frans Spaepen and Michael Falk for helpful discussions. The authors acknowledge primary financial support from the NSF MRSEC DMR-1119826 (KZ and MW) and partial support from NSF grant numbers DMR-1006537 (CO) and CBET-0968013 (MS).

Appendix A: Thermostat and Quenching Protocol

In this appendix, we provide additional details of the molecular dynamics (MD) simulations used to thermally quench Lennard-Jones (LJ) systems from high temperature liquids to low temperature glasses. The LJ liquids were first equilibrated at high temperature $T_0 = 2.0$ using constant number N , volume V , and temperature T MD simulations, and cooled exponentially $T(t) = T_0 e^{-Rt}$ to low temperature $T_f = 10^{-2}$. The temperature was controlled using the Nosé-Hoover thermostat [10, 11] with thermal inertia parameter $Q = 1$, and the equations of motion were integrated using a Newton’s method technique [27] with time step $\Delta t = 10^{-3}$. In Fig. 6 (left), we show for monodisperse LJ systems with $N = 4000$ that the dependence of the median local bond orientational parameter \bar{Q}_6^l on rate R is the same for $Q = 1$ and 10.

We also investigated the extent to which the thermostat affects the critical cooling rate, below which the sys-

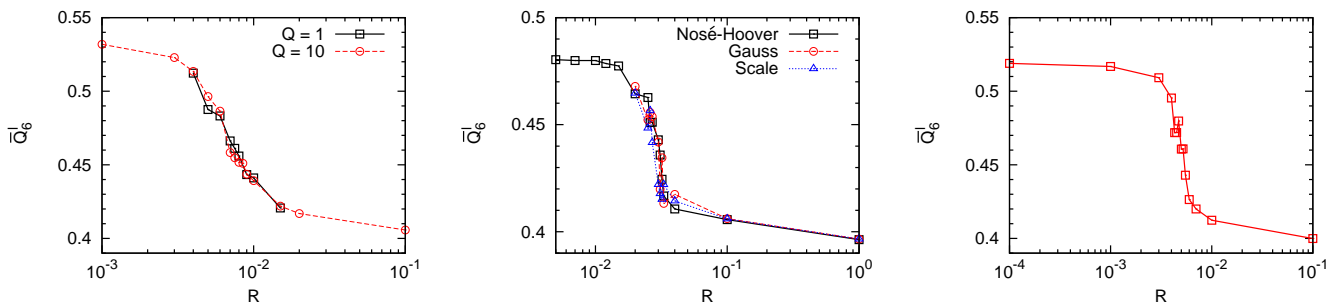


FIG. 6: (left) Median local bond-orientational order parameter \overline{Q}_6^l versus the cooling rate R for monodisperse LJ systems with $N = 4000$ using the Nosé-Hoover thermostat with thermal inertia parameter $Q = 1$ (\square) and 10 (\odot) in units of $m\sigma_{AA}^2$. (middle) Median local bond-orientational order parameter \overline{Q}_6^l versus R for monodisperse LJ systems with $N = 500$ using several thermostats: Nosé-Hoover (\square), Gaussian constraint (\odot), and *ad hoc* velocity rescaling \triangle . (right) Median local bond-orientational order parameter \overline{Q}_6^l versus the cooling rate R for monodisperse systems with $N = 1372$ for a linear thermal quenching protocol, $T(t) = T_0 - Rt$.

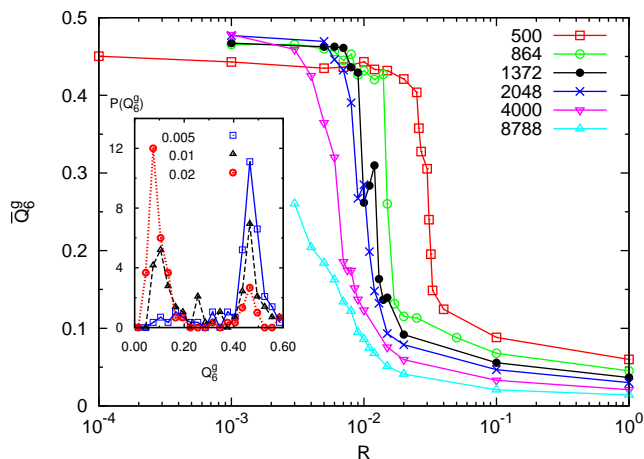


FIG. 7: (color online) Median global bond orientational order parameter \overline{Q}_6^g for monodisperse LJ systems following thermal quenches to $T_f = 0.01$ over a range of cooling rates R for system sizes $N = 500, 864, 1372, 2048, 4000,$ and 8788 . (inset) The probability distribution $P(Q_6^g)$ for monodisperse LJ systems with $N = 1372$ following quenches to $T_f = 0.01$ for cooling rates $R = 0.02$ (\circ), 0.01 (\triangle), and 0.005 (\square).

tems crystallize. In Fig. 6 (center), we show that \overline{Q}_6^l versus R is the same for monodisperse LJ systems with $N = 500$ when the temperature is controlled using the Nosé-Hoover, Gaussian constraint, and *ad hoc* velocity rescaling thermostats [8, 28]. Thus, the choice of the thermostat does not influence the measurement of R_c . We also varied the form of the thermal quenching protocol. In Fig. 6 (right), we show that a linear cooling schedule, $T(t) = T_0 - Rt$, gives qualitatively the same results for \overline{Q}_6^l versus R as an exponential temperature ramp.

Appendix B: Characterization of Crystalline Order

In this Appendix, we describe several metrics (in addition to the local bond orientational order parameter Q_6^l in Eq. 2) to characterize the degree of crystalline order of thermally quenched LJ systems. In contrast to Q_6^l , the global bond orientational order parameter Q_6^g in Eq. 3 quantifies the degree of crystallization over the entire system. The median global bond orientational order parameter \overline{Q}_6^g versus cooling rate R for monodisperse LJ systems for several system sizes is shown in Fig. 7. \overline{Q}_6^g shows a rapid increase near the critical cooling rate R_c as found for \overline{Q}_6^l . However, R_c (defined by a threshold such as $\overline{Q}_6^g = 0.3$) appears to decrease to zero in the large system limit. This trend occurs because it takes an increasing amount of time (and thus slower cooling rates) for crystal nuclei to grow and for the system to reach the same \overline{Q}_6^g as that obtained in smaller systems.

In Fig. 8 (left), we show the local bond orientational order correlation function (Eq. 4) for monodisperse LJ systems with $N = 1372$ for several cooling rates. We find that $G_6(r)$ plateaus at large r and the plateau value $G_6(\infty)$ increases with decreasing cooling rate R . For partially crystalline systems, $G_6(r)$ decays to $1/\sqrt{N_d}$ at large distances, where N_d is the number of independent crystalline domains. For disordered systems, $G_6(r)$ decays to $1/\sqrt{N_b}$, where N_b is the total number of nearest neighbor particles [13]. We find that the deviation $G_6(r_{\max}) - G_6(\infty)$, where $G_6(r_{\max})$ are the local maxima in $G_6(r)$, decays exponentially $\sim e^{-r/\xi}$ with correlation length ξ . (See Fig. 8.) The correlation length ξ grows linearly with the linear size of the system $N^{1/3}$ for cooling rates $R < R_c$.

We also employed a crystal analysis algorithm to identify the crystalline clusters (FCC, HCP [15], or BCC) that form during the thermal quenching process. For slow cooling rates, the system forms only a few large crystalline clusters whose size scales with the system size.

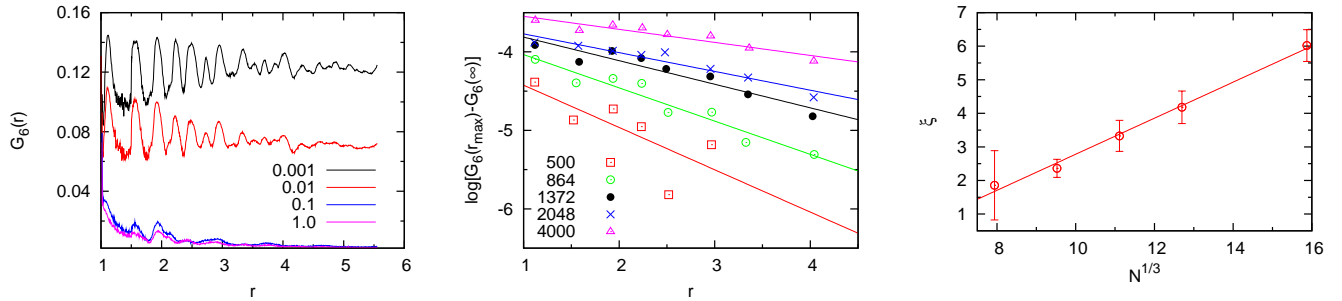


FIG. 8: (color online) (left) Local bond orientational order correlation function $G_6(r)$ for monodisperse LJ systems with $N = 1372$ at several cooling rates $R = 1, 10^{-1}, 10^{-2},$ and 10^{-3} . (middle) The decay of the local maxima in $G_6(r)$ versus distance r for monodisperse LJ systems at cooling rate $R = 10^{-3}$ for several system sizes $N = 500, 864, 1372, 2048,$ and 4000 . (right) Correlation length ξ from the decay of the local bond orientational order correlation function versus the linear dimension of the system $N^{1/3}$ for monodisperse LJ systems at cooling rate $R = 10^{-3}$. The solid line has slope ≈ 0.5 .

(See Fig. 9). For fast cooling rates, the number of crystalline clusters is small, and each cluster contains only a few particles. At intermediate rates, the number of crystalline clusters reaches a maximum at a characteristic cooling rate that scales with N as shown in Fig. 9.

These results are consistent with the fact that the critical cooling rate R_c (defined using the local bond orientational order parameter Q_6^l) becomes independent of the system size in the $N \rightarrow \infty$ limit.

-
- [1] G. Kumar, P. Neibecker, Y. H. Liu, and J. Schroers, *Nature Communications* **4**, 1536 (2013).
- [2] A. Inoue, *Acta Mater.* **48**, 279 (2000).
- [3] D. Turnbull, *Contemp. Phys.* **10**, 473 (1969).
- [4] A. Takeuchi and A. Inoue, *Mater. Trans.* **46**, 2817 (2005).
- [5] D. B. Miracle, W. S. Sanders, and O. N. Senkov, *Philos. Mag.* **83**, 2409 (2003).
- [6] P. Jalali and M. Li, *Intermetallics* **12**, 1167 (2004).
- [7] P. Jalali and M. Li, *Phys. Rev. B* **71**, 014206 (2005).
- [8] M. P. Allen and D. J. Tildesley, *Computer Simulation of Liquids* (Oxford University Press, New York, 1987).
- [9] A. B. Hopkins, Y. Jiao, F. H. Stillinger, and S. Torquato, *Phys. Rev. Lett.* **107**, 125501 (2011).
- [10] S. Nose, *J. Chem. Phys.* **81**, 511 (1984).
- [11] W. G. Hoover, *Phys. Rev. A* **31**, 1695 (1985).
- [12] P. J. Steinhardt, D. R. Nelson, and M. Ronchetti, *Phys. Rev. B* **28**, 784 (1983).
- [13] C. F. Schreck and C. S. O'Hern, in *Experimental and Computational Techniques in Soft Condensed Matter Physics*, edited by J. Olafsen (Cambridge University Press, Cambridge, 2010), pp. 25–61.
- [14] Y. T. Wang, S. Teitel, and C. Dellago, *J. Chem. Phys.* **122**, 214722 (2005).
- [15] A. Stukowski, *Modelling Simul. Mater. Sci. Eng.* **20**, 045021 (2012).
- [16] HCP-like particles and clusters reported in this work are identified by considering the first nearest neighbors of each particle. If instead, the super-lattice across stacking layers was included, most of the HCP clusters would be classified as ‘9R’ structures [29] (with repeating motifs composed of an FCC layer followed by two HCP layers).
- [17] M. D. Rintoul and S. Torquato, *Phys. Rev. Lett.* **77**, 4198 (1996).
- [18] J. D. Honeycutt and H. C. Andersen, *Chem. Phys. Lett.* **108**, 535 (1984).
- [19] J. D. Honeycutt and H. C. Andersen, *J. Phys. Chem.* **90**, 1585 (1986).
- [20] A. R. Miedema, R. Boom, and F. R. Deboer, *J. Less-Common Met.* **41**, 283 (1975).
- [21] R. Boom, F. R. de Boer, and A. R. Miedema, *J. Less-Common Met.* **45**, 237 (1976).
- [22] R. Boom, F. R. de Boer, and A. R. Miedema, *J. Less-Common Met.* **46**, 271 (1976).
- [23] J. H. O. Varley, *Philos. Mag.* **45**, 887 (1954).
- [24] Y. Q. Cheng, E. Ma, and H. W. Sheng, *Phys. Rev. Lett.* **102** (2009).
- [25] X. J. Liu, X. D. Hui, G. L. Chen, and T. Liu, *Phys. Lett. A* **373**, 2488 (2009).
- [26] O. N. Senkov, Y. Q. Cheng, D. B. Miracle, E. R. Barney, A. C. Hannon, and C. F. Woodward, *J. App. Phys.* **111**, 123515 (2012).
- [27] D. Frenkel and B. Smit, *Understanding Molecular Simulation* (Academic Press, 2002).
- [28] D. Brown and J. H. R. Clarke, *Mol. Phys.* **51**, 1243 (1984).
- [29] F. Ernst, M. W. Finnis, D. Hofmann, T. Muschik, U. Schönberger, and U. Wolf, *Phys. Rev. Lett.* **69**, 620 (1992).

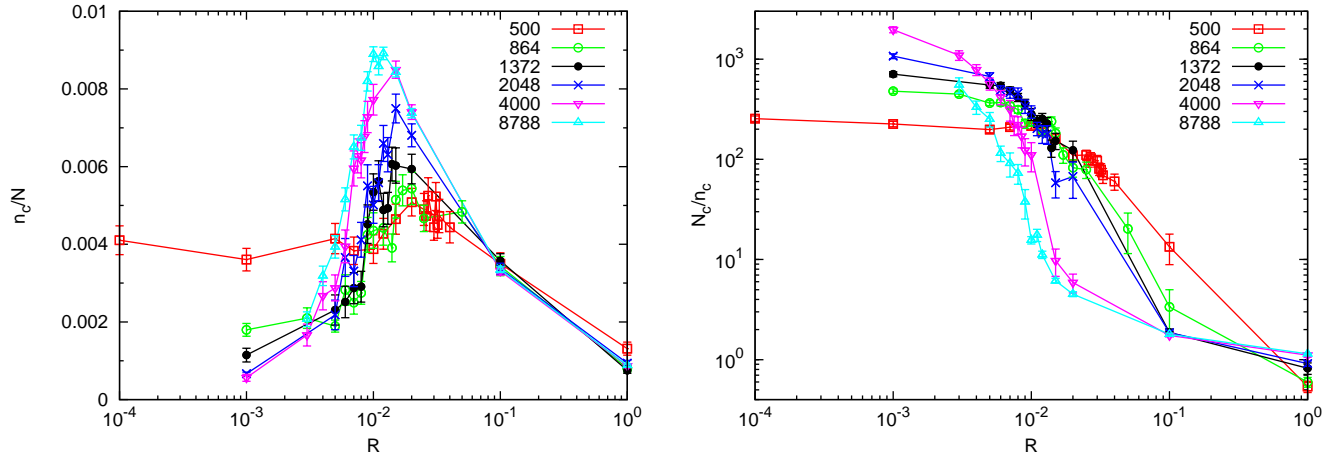


FIG. 9: (color online) (left) The number of crystalline clusters n_c (FCC, HCP, and BCC) normalized by the system size N for monodisperse LJ systems as a function of cooling rate R for several system sizes. (right) The number of (FCC, HCP, and BCC) crystal-like particles N_c normalized by the number of crystalline clusters n_c (*i.e.* average crystalline cluster size) as a function of cooling rate for several system sizes.